HHS Public Access

Author manuscript

J Mol Biol. Author manuscript; available in PMC 2015 March 17.

Published in final edited form as:

J Mol Biol. 2010 August 13; 401(2): 194–210. doi:10.1016/j.jmb.2010.06.019.

Regulatory insertion removal restores maturation, stability and function of ΔF508 CFTR

Andrei A. Aleksandrov[2,5], **Pradeep Kota**[1,3], **Luba A. Aleksandrov**[1,5], **Lihua He**[1,5], **Tim Jensen**[1,5], **Liying Cui**[1,5], **Martina Gentzsch**[4,5], **Nikolay V. Dokholyan**[1,3], and **John R. Riordan**[1,5,*]

[1] Department of Biochemistry and Biophysics, University of North Carolina-Chapel Hill, Chapel Hill, NC 27599, USA

[2] Department of Biomedical Engineering, University of North Carolina-Chapel Hill, Chapel Hill, NC 27599, USA

[3] Department of Molecular and Cellular Biophysics Program, University of North Carolina-Chapel Hill, Chapel Hill, NC 27599, USA

[4] Department of Cell and Development Biology, University of North Carolina-Chapel Hill, Chapel Hill, NC 27599, USA

[5] Cystic Fibrosis Treatment and Research Center, University of North Carolina-Chapel Hill, Chapel Hill, NC 27599, USA

Abstract

The cystic fibrosis transmembrane conductance regulator (CFTR) epithelial anion channel is a large multi-domain membrane protein which matures inefficiently during biosynthesis. Its assembly is further perturbed by the deletion of F508 from the first nucleotide binding domain (NBD1) responsible for most cystic fibrosis. The mutant polypeptide is recognized by cellular quality control systems and is proteolyzed. CFTR NBD1 contains a 32 residue segment termed the regulatory insertion (RI) not present in other ABC transporters. We report here that RI deletion enabled ΔF508 CFTR to mature and traffic to the cell surface where it mediated regulated anion efflux and exhibited robust single chloride channel activity. Long term pulse-chase experiments showed that the mature ΔRI/ΔF508 had a $T_{1/2}$ of ~14h in cells, similar to the wild-type. RI deletion restored ATP occlusion by NBD1 of ΔF508 CFTR and had a strong thermo-stabilizing influence on the channel with gating up to at least 40°C. None of these effects of RI removal were achieved by deletion of only portions of RI. Discrete molecular dynamics simulations of NBD1 indicated that RI might indirectly influence the interaction of NBD1 with the rest of the protein by attenuating the coupling of the F508 containing loop with the F1-like ATP-binding core

*To whom correspondence should be addressed: jack_riordan@med.unc.edu, 6103 Thurston Bowles Bldg., CB#7248, Chapel Hill, NC 27599, USA, Phone: (919) 966- 0329, FAX: (919) 966-5178.

subdomain so that RI removal overcame the perturbations caused by F508 deletion. Restriction of RI to a particular conformational state may ameliorate the impact of the disease-causing mutation.

Keywords

ABC transporters; CFTR; cystic fibrosis; ion channel; DMD simulations

Introduction

CFTR is a hydrolyzable-ligand gated ion channel which employs the ABC transporter structural architecture to couple ATP binding and hydrolysis with its anion channel activity [1]; [2]. Although a very large number (~1600) of different mutations in the CFTR gene have been identified in patients with cystic fibrosis, a single mutation (ΔF508) is present on at least one allele in 90% of patients (http://www.genet.sickkids.on.ca/cftr/app). The deletion of the F508 residue from the N-terminal nucleotide binding domain (NBD1) of CFTR prevents normal folding and assembly of the protein so that it is recognized as abnormal by quality control systems and cleared from both the early and late secretory pathways. However under certain conditions where the mutant molecule is able to avoid this fate, it is at least partially functional as an anion channel at the cell surface [3]. These conditions include maintenance of cells expressing the protein at low temperature [4] and exposure to osmolytes [5] or certain small molecules either binding to the protein or acting on the cellular quality control apparatus [6]; [7]. There are also a number of second site amino acid substitutions that partially restore conformational maturation, intracellular trafficking and function of ΔF508 CFTR [8]; [9]; [10]. Thus development of means to overcome or circumvent the effect of the F508 deletion would provide an important therapeutic strategy for treatment of the disease. Increased understanding of the nature of the disruption of the molecule caused by the absence of F508 is necessary for the implementation of such strategies. For example the finding that the absence of F508 from the surface of NBD1 perturbs its interaction with a cytoplasmic loop (CL4) in the C-terminal membrane spanning domain (MSD2) has focused attention on this interface between domains as a target of stabilizing small molecules [11].

While the overall 3D structure of the isolated NBD1 as determined by X-ray crystallography is not altered by the ΔF508 mutation [12], both the folding yield [13] and pathways [14] of the domain are different from those of the wild-type. A unique feature of CFTR NBD1 relative to the NBDs of all other ABC proteins is the insertion of a 32 residue segment between the first two beta strands in the structure of the domain [15]. The role of this extra polypeptide, which has been termed the Regulatory Insertion (RI), in CFTR structure and function is unknown as deletion of most of it including the PKA phosphorylation site at serine 422 apparently has little effect on the expression and channel function of wild-type CFTR in *Xenopus* oocytes [16]. However, very recently it was shown that complete RI deletion promotes homodimer formation and stability of NBD1 with only minor structural changes upon F508 deletion [17]. We hypothesized that the absence of the RI might improve stability of full-length ΔF508 CFTR expressed in mammalian cells. We found that unlike the influence of many mutations in NBD1, deletion of the complete RI sequence did not impair

expression and processing of wild-type CFTR but on the contrary promoted the maturation of ΔF508 CFTR. Not only did the RI deleted ΔF508 CFTR escape ER quality control and reach the Golgi apparatus to acquire complex oligosaccharide chains but it also was stabilized at the cell surface where it mediated robust chloride channel activity. Discrete molecular dynamics simulations showed that coupling between the dynamics of the F508 containing loop and the F1-like ATP-binding core subdomain of NBD1 disappeared upon F508 deletion. Furthermore there was a dramatic increase in the flexibility of the structurally diverse region (SDR) involved in contacts of NBD1 with the first cytoplasmic loop (CL3) in the C-terminal membrane spanning domain. Both changes were at least partially overcome by RI deletion. Overall, our findings reveal that the presence of the functionally non-essential RI is a major contributor to the structural and functional instability of ΔF508 CFTR.

Results

RI deletion enables ΔF508 CFTR maturation and traffic to the cell surface

The structure and position of RI as seen in the X-ray structure of mouse NBD1 is shown in Fig. 1 with alpha helical elements at both ends and a very short helix containing the serine 422 PKA phosphorylation site in the middle. Although the deletion of the last two thirds of the segment has been found to have little effect on channel activity in *Xenopus* oocytes [16] we postulated that the presence or absence of the entire large peptide insertion might have some influence on the assembly and stability of the molecule. Since the ΔF508 mutation strongly influences both of these parameters we tested the effect of RI removal on the behavior of ΔF508 CFTR in mammalian cells. Strikingly, the complete RI deletion resulted in very substantial maturation of ΔF508 CFTR when expressed transiently in HEK 293 cells or stably in BHK cells as evidenced by appearance of the more slowly migrating band in Western blots (Fig 2). Quantification of the band intensities indicated that the steady-state amount of the ΔRI/ΔF508 more slowly migrating mature form was approximately one-third that of the wild-type in the 293 cells (Fig 2b). Maturation of ΔRI/ΔF508 CFTR also occurred in other cell types including BHK cells (Fig 2c) and was enriched in their isolated membranes (Fig 2d). That the mature band contained complex N-linked oligosaccharide chains added in the Golgi apparatus is shown by its sensitivity to N-glycanase but not to endoglycosidase-H (Fig 2e). Thus while the degree of maturation of ΔF508 is still considerably less than that of the wild-type it is comparable to or exceeds that resulting from other means of rescue including growth of cells at low temperature, suppressor or solubilizing single residue substitutions in NBD1 or small corrector molecules [7]; [18]. Estimation of the amount of ΔRI/ΔF508 CFTR that reaches the cell surface is described below. The maturation of ΔF508 CFTR was achieved only by deletion of the entire RI fragment, as deletion of just the N-terminal or C-terminal portion did not have this effect (Fig 2f). Although we have not studied the influence of RI deletion on wild-type CFTR in detail, its maturation also was augmented as clearly indicated in Fig S1.

To determine whether removal of RI had stabilized ΔF508 CFTR in terms of its lifetime in the cell, long term pulse-chase experiments were performed. As seen in Fig 3a, mature ΔRI/ΔF508 decayed at a rate similar to wild-type CFTR indicating that there had been substantial

stabilization of the mutant protein which, when unmodified, decays very rapidly [19]. As might be expected from the amount of mature ΔRI/ΔF508 protein, much of it is localized to the cell surface as can be seen by immunofluorescence staining (Fig 3b, left upper panels). The plasma membrane pool is particularly well delineated after cells have been treated with cycloheximide so that the intracellular pool of immature protein is depleted (Fig 3b, left lower panels). Under these conditions it was possible to quantify the intensity of the cell surface fluorescence due to immunostaining of ΔRI/ΔF508 relative to wild-type CFTR (Fig 3b, right panel). By these estimates the density of the restored mutant protein on the cell surface was approximately 60% of that of the wild-type. This proportion is larger than that of the mature protein bands in the two cell types in Western blots (Fig 2), possibly suggesting that the surface pool may be stabilized more than the total post-ER pool with complex oligosaccharide chains. Alternatively, the difference between the ~30% and ~60% estimates may largely reflect differences between the two methods.

There is little or no ΔF508 CFTR protein at the surface of stably expressing BHK cells grown at 37°C. Accordingly, there is a barely detectible cyclic AMP stimulated iodide efflux response by these cells (Fig 3c, left panel). However, with cells expressing ΔF508 CFTR from which the RI has been deleted, efflux is strongly stimulated when cellular cyclic AMP is increased (Fig 3c, dotted line). While the response is significantly delayed compared to that of cells expressing wild-type CFTR, the overall magnitude is similar. This result provides evidence that the ΔRI/ΔF508 protein that is able to traffic to the cell surface is functional. In addition, when the relative single channel properties of ΔRI/ΔF508 and wild-type CFTR are taken into account (see Figs 7 and 8) the cumulative efflux data (Fig 3c, right panel) also provide an estimate of the relative amounts of active protein in the plasma membrane. Since the slopes of those efflux curves differ by a factor of 4 while the open probability of ΔRI/ΔF508 at 25°C is approximately one-half that of the wild-type, the number of rescued mutant CFTR channels should be approximately half of the wild-type in general agreement with the estimates by the other two methods.

RI deletion restores the ability of ΔF508 CFTR to bind and trap ATP at NBD1

The first ATP binding site in CFTR occludes but does not hydrolyze ATP whereas the second site is hydrolytic [20]; [21]. This behavior is reflected by the fact that $8N_3$ATP is stably bound to NBD1 prior to its covalent attachment by photoactivation whereas the nucleotide bound to NBD2 may rapidly dissociate. $8N_3[\gamma^{32}P]$ATP bound to defined NBD containing fragments produced by limited proteolytic digestion is readily detected and quantified by autoradiography after SDS-PAGE. Thus after incubation of CFTR containing membranes with $8N_3[\gamma^{32}P]$ATP, the products of hydrolysis are readily washed away from NBD2 while the unhydrolyzed nucleotide is retained at NBD1 (Fig 4a, WT). Although at 4°C there is weak nucleotide binding to NBD1 of temperature rescued ΔF508 CFTR, this binding does not withstand washing, indicating that it is not trapped as in the wild type (Fig 4a, ΔF508). In ΔRI/ΔF508 CFTR the trapping of the nucleotide is restored, making it resistant to washing from NBD1. The detection of the bound nucleotide in a larger NBD1 containing tryptic fragment (~70kDa) when RI is deleted, compared with a fragment of ~40kDa when it is present, is due to the removal of a trypsin cleavage site within the RI [22]. This difference is also evident in the RI deleted wild-type (Fig 4a, RI). The data in Fig 4a clearly show that the

ability of wild-type NBD1 to stably trap the nucleotide, which is lost in ΔF508, is reestablished by deletion of RI.

The weak nucleotide binding to NBD1 of temperature rescued ΔF508 CFTR completely disappeared when the temperature of the CFTR containing membranes was increased from 4°C to 35°C (Fig 4b, right two lanes). Importantly, when RI was deleted the ability of ΔF508 CFTR to retain the nucleotide at 35°C was completely restored (Fig 4b, middle two lanes), as in the wild type CFTR (Fig. 4b, left two lanes). These results substantiate those in Fig 4a and emphasize the capacity of RI removal to compensate for the effect of the ΔF508 mutation on the ability of NBD1 to trap ATP.

Further evidence of the restored ability of ΔRI/ΔF508 to retain ATP bound at NBD1 is shown in Fig 4c and d where the slow rate of dissociation at 35°C is very similar to that of the wild-type with a $T_{1/2} > 30$ minutes [23]. Thus in addition to extending the life time of ΔF508 CFTR protein to the same range as that of the wild-type, RI deletion also restored the capacity of ΔF508 NBD1 to bind and occlude ATP to a very similar extent as wild-type.

RI deletion restores cross-linking of domain interfaces in ΔF508 CFTR

The ΔF508 mutation disrupts inter-domain contacts in CFTR including those so-called domain-swapping interactions between sites on either NBD and cytoplasmic loops in membrane-spanning domains on the opposite side of the molecule[11]; [24]. To determine if these interfacial contacts are restored on deletion of RI, pairs of cysteine residues were introduced at these locations in Cys-less ΔF508 CFTR constructs in which RI was either present or absent (Fig 5). Treatment of cells expressing these constructs with bifunctional methane-thiosulfonate reagents resulted in cross-linking of members of both these cysteine pairs when RI had been removed, indicating reestablishment of native-like contacts between NBD2 and CL2 as well as NBD1 and CL4. Thus RI removal from ΔF508 NBD1 brings about the restoration of disrupted interactions between domains throughout the molecule.

RI deletion restores stable ΔF508 CFTR channel activity

The cAMP stimulated iodide efflux from ΔRI/ΔF508 CFTR expressing cells (Fig 3c) indicated its functional capability. However, single channel gating provides the most sensitive measure of CFTR function. When ΔF508 CFTR molecules reach the surface of cells grown at reduced temperature or treated with osmolytes or so-called corrector small molecules, attenuated channel activity is observed [25–28]. When assayed at room temperature this activity persists, at least during the periods of the assays, but is lost very rapidly at physiological temperature [27]; [29]; [30]. This behaviour is detailed in Fig 6 for channels in membranes of ΔF508 CFTR expressing cells grown at 27°C and treated with correctors VRT-325 and Corr-4a in combination (see Fig 9). The heterogeneous nature of the gating kinetics is immediately apparent from visual inspection of 10 minutes of recording at +25°C (Fig 6a). The reversible inter-conversion between patterns of activity with two different conductances is confirmed by two well defined peaks (10.6±0.4 pS and 6.1±0.6 pS) for the open states in the all points histogram shown on the left. The fact that both conductive states belong to the same functional unit is confirmed by the absence of their superposition in these records with hundreds of transitions between open and closed states as well as direct gradual

inter-conversion between distinct open states (not shown). The latter are very rare events and in the most cases, inter-conversion proceeds in the closed state. The patterns of activity persist long enough to be easily separated for further analysis. However, the problem of ΔF508 CFTR non-stationary gating kinetics for the patterns with fully open state precludes kinetic analysis with a high degree of confidence [27]. At least three different patterns of activity do occur at +25°C as shown in Fig 5b,c,d. The patterns of activities shown in Fig 5b,c have conductance of 10.6 pS and P_o values progressively decreasing in time from the nearly wild-type value of 0.26 at the beginning to the low 0.04 value between 6 and 8 minutes of recording for the experiment shown in Fig. 6a. In different experiments the overall P_o for the full open state conductance may vary from 0.26 to 0.04. Only the activity shown in Fig 6d with a stable sub-conductance level of 6.1 pS and P_o= 0.52 remains after 15 minutes at +25°C.

The single channel activity exhibited at +35°C is shown in Fig. 6e where the only peak in the all points histogram is that of the stable closed state. No stable open states occur at this temperature but some unresolved brief openings could result in a leak current in whole-cell recordings. Further progressive loss of activity occurs as temperature is ramped from +35°C to +40°C (Fig 5f) with the closed state predominant at +40°C where only very rare and brief unresolved openings are visible (Fig 6g).

Examination of the single channel properties of ΔRI/ΔF508 CFTR using the same experimental protocols showed very different results (Fig 7). First unlike the unmodified ΔF508, stable activity was observed at 25°C with homogeneous full conductance openings (Fig 7a). The open probability of 0.12 was approximately half that of the wild-type under the same conditions (see Fig 8a). Recording at 35°C, where virtually no stable openings of ΔF508 channels could be detected, revealed uniform gating transitions having an open probability only ~20% less than wild-type and with identical conductance (compare Fig 7b and 8b). Most striking, during continuous temperature increase from 35°C to 40°C, gating persisted and accelerated with the expected increase in conductance (Fig 7c). This behavior mimicked that of the wild-type (Fig 8c) as did the persistent stable gating when the channels were held at 40°C for prolonged periods (compare Figs 7a and 8a). These data emphasize that the major impact of the removal of the complete RI from ΔF508 CFTR is to overcome the functional failure of the channel in the physiological temperature range caused by F508 deletion.

RI deletion increases the sensitivity of ΔF508 to small molecule correctors

To investigate the relationship of RI deletion to other manipulations that promote maturation of ΔF508 we tested the effects of both the growth of cells at reduced temperature and exposure to small molecule corrector compounds [7]; [31]. As seen in Fig 9, a small amount of mature band C appeared in cells expressing ΔF508 CFTR grown at 27°C (lane 5) and this was greatly increased on simultaneous exposure to the two corrector compounds, Corr-4a and VRT-325 (lane 6). However, at 37°C, there was only a very modest response to the two compounds (compare lanes 11 and 12). This is consistent with the general experience that these compounds are much more effective at lower than at higher temperature. With the RI deleted ΔF508 however, the effects of low temperature and these corrector compounds

separately or together appeared to be quite different. First, the degree of maturation of ΔRI/ΔF508 (amount of band C) was fairly similar at 27°C (lane 1) and 37°C (lane 7), indicating that when the RI is not present the temperature sensitivity of the ΔF508 mutant is reduced. Second, compound VRT-325 alone caused a similar further increase in maturation of ΔRI/ΔF508 at both temperatures (lanes 2 and 8). While of lesser magnitude, the stimulation caused by Corr-4a also was not greatly different at the two temperatures (lanes 3 and 9). More striking was the influence of the two compounds acting together where the extent of maturation was as great at 37°C (lane 10) as at 27°C (lane 4) and in the same range as the wild-type. As already noted, this degree of correction of ΔF508 containing the RI by the two compounds is only possible at the lower temperature (lane 6). Thus these observations are consistent with the idea that the presence of the RI contributes substantially to the thermo-sensitivity of the ΔF508 polypeptide. The fact that the effects of RI removal and at least these two correctors are distinct and additive, whereas there is some commonality to the effects of RI deletion and low temperature, suggests that these compounds do not act at the level of the RI and is consistent with RI influencing the thermodynamic stability of the protein.

Influence of RI on NBD1 dynamics

The rescue of ΔF508 by the deletion of the RI region suggests a potential dynamic coupling between the RI region and the F508 containing segment. Mutations in other sites in NBD1, such as the W496[19], F494/Q637 (25), and F429/F494/Q637[8], partially attenuate the trafficking and gating defect of the full-length ΔF508 CFTR. The mechanism by which RI deletion and single residue substitutions within NBD1 rescue ΔF508 is unknown. However these observed compensatory effects suggest the plausible hypothesis that these regions may be dynamically coupled. To investigate this possibility, we performed discrete molecular dynamics (DMD) simulations [32]; [33] of both wild type and ΔF508 NBD1 with and without the RI. In order to determine the conformational flexibility of NBD1, we computed the root-mean-square fluctuations (RMSF) for each amino acid in NBD1 for all the NBD1 constructs during the course of a simulation (Fig 10a). We find that the RI region is indeed flexible and dynamic, which is in agreement with the observed elevated b-factors in the NBD1 crystal structures [15] and NMR studies [34]. This flexibility of RI in wild-type CFTR NBD1 is comparable to that in ΔF508 CFTR NBD1. However, the structurally diverse region L526-T547 (SDR) of the domain [35]; [36] containing residue I539, one of the sites targeted for rescue of the ΔF508 defect [10], shows increased flexibility in the ΔF508 background, compared to WT CFTR NBD1 with maximum difference in the RMSF values at residue E543. After RI deletion the flexibility of this region is restored to the wild-type level. In view of these results, we propose that the flexibility of the RI region is dynamically coupled to the SDR region, suggesting that deletion of the RI region is equivalent to incorporating restorative mutations at this and other sites.

In order to further evaluate the probable dynamic coupling of distant sites in CFTR-NBD1, we performed covariance analysis (see methods) on the entire domain (Fig. 10b). In our analyses, if two sites in NBD1 move in concert, even if sequentially and spatially distant from each other, the sites are considered to be correlated. We observed that the dynamics of the F508 containing loop is coupled to that of the SDR (Fig 10b) both of which have been

hypothesized to participate in formation of the interface with the cytoplasmic loops (CL3 and CL4) in MSD2[11]; [24] and this coupling was not strongly affected by F508 deletion. We constructed normalized correlation maps for NBD1 from the simulation trajectories to estimate coupling between different regions of NBD1. Each correlation map is an N×N covariance matrix (where N is the length of the protein) of correlation coefficients derived from the simulation trajectory. The covariance matrix describes the correlation of the positional fluctuations of α carbon atoms of different residues in NBD1. The correlation coefficient ranges from −1 to 1 where a value of 1 represents strong positive correlation (red dots in Fig. 10b) while a value of −1 denotes strong negative correlation (blue dots in Fig. 8b). We find that the dynamics of the loop containing F508 and the RI region are not coupled in the wild type NBD1 (yellow region in Fig. 10b). However, the F508 containing loop demonstrates strong correlations in dynamics with the F1-like ATP binding core subdomain (blue dots in Fig 10b). These correlations were completely lost upon F508 deletion and were at least partially restored upon removal of the RI region (Fig 10b). This observation suggests the possibility that the RI region may regulate the coupling of movements of the F508 containing segment with the F1-like ATP binding core subdomain of NBD1. In light of the fact that the structure of NBD1 is not significantly different with and without F508[35], we hypothesize that it is not the structure but the dynamics of NBD1 that has the greater influence on CFTR trafficking, maturation and function.

Discussion

The way in which the absence of a single residue (F508) compromises the CFTR molecule in most patients with cystic fibrosis has remained incompletely understood. The end result of the mutation is that, although fully synthesized at a normal rate, most of the nascent polypeptide is ubiquitinylated and succumbs to proteasomal degradation at the endoplasmic reticulum [37]; [38]. Much has been learned about how the quality control apparatus appraises and culls the aberrantly assembled molecules both co- and post-translationally [39]; [40]. Manipulation of different components of this apparatus including multiple molecular chaperones has been attempted as a means of improving the maturation of ΔF508 CFTR. In one case, down-regulation of the Hsp90 co-chaperone, Aha-1 had at least a partial positive effect [41] and efforts of this type are continuing. Some of the small molecules turned up in cell-based high through-put screens probably act on constituents of the biosynthetic processing and quality control systems as they are not entirely specific for CFTR. Other so-called correctors may bind directly to CFTR but as yet there is limited evidence supporting this hypothesis[42]. Understanding of the mechanism of action of this latter group of small molecules and the development of improved ones is impaired by the fact that the exact influence of the lack of F508 on the CFTR protein is still unclear. While it has become apparent that the absence of the residue from the surface of NBD1 precludes its normal interaction with the last cytoplasmic loop in the C-terminal membrane spanning domain [11], the extent of perturbation elsewhere in the molecule is less evident. Comparison of the X-ray structures of isolated wild-type and ΔF508 NBD1 showed that the overall fold was unaltered [12]. A more recent extensive analysis of structures of multiple wild-type and mutant NBD1s with or without several solubilizing substitutions confirmed that differences were restricted to the small F508 containing surface patch although several other surface regions appeared

to be quite mobile in all of these structures [35]. The same study, using hydrogen/deuterium exchange measurements to address structural dynamics of the domain, essentially confirmed the crystallography findings. Nevertheless, it is known that second site substitutions of residues at locations quite separate from F508 can compensate for the effects of its deletion [35]. These findings indicate that specific structural features of the domain do determine the impact of the mutation.

Although shown not to be essential to CFTR channel function [16], the RI is a unique feature of NBD1 and in the current study we have determined that it strongly influences the impact of the ΔF508 mutation. First, we confirmed that, in mammalian cells, as in *Xenopus* oocytes, RI is not essential to the biogenesis, stability and function of wild-type CFTR. In fact, the steady state amount of the RI deleted protein in transiently transfected HEK cells is greater than that of the wild-type CFTR (Fig. 2a and S1). While our preliminary single channel analysis indicates that gating may be somewhat slowed, open probability is not greatly reduced. The effects of RI removal on ΔF508 CFTR were much more pronounced. Maturation was increased to a level at least one third that of the wild-type and those molecules that did mature were very active with open probability not much less than wild-type (Figs 7 and 8). Even more impressive was the stability of the ΔRI/ΔF508 protein in terms of both its lifetime in cells and its channel activity at elevated temperature. The rate of turnover of the mutant mature form was not less than that of the wild-type (Fig 3a) and robust channel gating persisted at temperatures up to at least 40°C (Fig 7). This increased thermostability of the channel, consistent with that observed with isolated NBD1[17], is especially notable because it has not been observed with other manipulations to rescue ΔF508 such as growth of cells at reduced temperature or in the presence of known correcting small molecules.

In addition to stabilization of channel activity, RI deletion also restored the ability of ΔF508 CFTR to bind and occlude ATP at NBD1 up to 35°C (Fig 4). This effect is consistent with the increased nucleotide binding affinity of isolated NBD1 from which RI was removed[17] and shows that RI, although located proximal to the bound nucleotide, is not necessary for occlusion.

Our experimental data do not explain how the RI segment of NBD1, far separated from F508 in the structure, has such a strong influence on the mutant protein. However, computational analysis of NBD1 dynamics revealed a dynamic correlation between the F508 containing loop and the F1-like ATP binding core subdomain (Fig 10), suggesting a coupling between them which is completely absent in the ΔF508 mutant. The ability to restore this coupling in the ΔF508 CFTR upon RI deletion is consistent with the possibility that RI attenuates this process by interaction with the F1-like ATP-binding core subdomain. Since the 507–511 loop is involved in the formation of the NBD1-CL4 interface [11] in full-length CFTR (Fig 10d), RI might indirectly influence the interaction of NBD1 with the rest of the protein by attenuating the coupling of the 507–511 loop with the F1-like ATP-binding core subdomain of NBD1.

Considering the strong influence of RI on the processing and stability of ΔF508 CFTR together with the likelihood that the peptide may normally assume different conformational

states within the complete CFTR molecule [34]; [43], one might postulate that restriction to one of these states would improve maturation of the mutant protein. Conceivably this might be achieved by the binding of a specific ligand targeted to the peptide. The possible utility of such reagents in combination with existing partially effective small molecules [44] that presumably act at other sites is illustrated by the fact that the latter are much more effective when RI is absent (Fig 9). Combination of an RI restricting agent with existing correctors might be anticipated to have similar additive effects. Related to the idea of combining different modulating agents, it should not be expected that the RI is solely responsible for the sensitivity of CFTR to the ΔF508 mutation because the related ABC transporters, P-glycoprotein and MRP1, lacking RI, also are misprocessed when an aromatic residue in the counterparts of the F508 position is deleted [45]; [46].

We focused primarily on the impact of RI on ΔF508 CFTR rather than the wild-type because of the potential practical significance of being able to positively impact the mutant. However, the functional role of RI in the wild-type protein still seems somewhat enigmatic since despite its presence in all species where CFTR is expressed, it is not essential to chloride channel activity [16]. More extensive studies are required to reveal the advantage of RI to wild-type CFTR function. As yet we have not definitively determined whether the wild-type CFTR channel's thermo-stability is further increased when RI is not present.

In summary, while the exact functional role of the unique RI in NBD1 of wild-type CFTR remains to be elucidated, we have found that it is a major contributor to the instability and dysfunction of ΔF508 CFTR responsible for most cystic fibrosis and as such may be a target for therapeutic agents which would diminish these effects.

Materials and methods

Materials

Mouse monoclonal CFTR antibodies to epitopes in the N-terminus (mAb13-4), R domain (mAb570) and NBD2 (mAb596) were generated as described [47]. Goat anti-mouse IgG-IR800 was from LiCor Corp. (Lincoln, NE), and goat anti-mouse IgG-AlexaFluor 488 was from Invitrogen (Carlsbad, CA). Small molecule correctors VRT-325 (4-Cyclohexyloxy-2-{1-[4-(4-methoxy-benzensulfonyl)-piperazin-1-yl]-ethyl}-quinazolin) and Corrector-4a (N-[2-(5-Chloro-2-methoxy-phenylamino)-4′-methyl-[4,5′]bithiazolyl-2′-yl]-benzamide) were generously provided by the Cystic Fibrosis Foundation.

CFTR construction and expression

The ΔRI/ΔF508 CFTR comprises human wild type CFTR protein with residues 404–435 and 508 deleted. Human CFTR cDNAs encoding wild-type or mutant proteins were expressed transiently in human embryonic kidney (HEK293) cells, or stably in baby hamster kidney (BHK-21) cells, with pcDNA3 and pNUT vectors, respectively as described previously [24]. ΔRI/ΔF508 CFTR constructs in pcDNA3 and pNUT vectors were generated from human wild type CFTR cDNA using the Quick Exchange protocol (Stratagene) as described, and sequences were confirmed by automated DNA sequencing (UNC-CH Genome Analysis Facility). Transfection was carried out using jetPEI transfection reagent

(Fermentas, Glen Burnie, MD) according to the manufacturer's instructions. For stable cell line establishment, BHK cells expressing CFTR were selected and maintained in methotrexate containing media as previously described [48].

Western blot and immunofluorescence microscopy

HEK or BHK cells overexpressing CFTR were harvested in RIPA buffer without SDS (50 mM Tris, 150 mM NaCl, 1% Triton X-100, 1% deoxycholate, pH 7.4) plus protease inhibitor cocktail (1 μg/ml leupeptin, 2 μg/ml aprotinin, 3.57 μg/ml E64, 156.6 μg/ml benzamidine and 2 mM Pefablock), and equal amounts of proteins in SDS-PAGE sample buffer were subjected to 7.5% SDS-PAGE and Western blot analysis with mAb596 to determine CFTR expression and maturation [22].

To determine the subcellular distribution of CFTR, BHK-21 cells grown in glass bottom culture dishes (MatTek Corporation) were fixed with 4% paraformaldehyde, permeabilized with 0.1% saponin, blocked with 1% bovine serum albumin and 5% normal goat serum. CFTR localization was detected by mAb570 in combination with Alexa Fluor 488 conjugated goat-anti-mouse IgG using a Zeiss LSM510 confocal laser scanning microscope.

Metabolic Pulse-chase labeling

BHK cells stably expressing wild-type and mutant CFTR were pulsed labeled with [^{35}S]-methionine and chased as previously described [49]. Briefly, BHK cells expressing wild type protein or ΔF508/ΔRI were grown to 80% confluency in 60 mm dishes. Cells were then labeled with 100 μCi per plate ^{35}S-methionine (Perkin Elmer, >1000Ci/mmol) for 8 hours in a cocktail of 90% methionine free medium, 10% normal growth medium and 10% FBS. After labeling, cells were washed 2 times with PBS and chased using growth medium supplemented with 1mM cold methionine. At the end of the chase period, cells were washed 2 times with PBS and solubilized with 1 ml RIPA buffer containing protease inhibitors. CFTR was immunoprecipitated using antibody 596 and Protein A beads (Invitrogen). Gels were fixed in 10% acetic acid/30% methanol, washed in water, then soaked in 1M sodium salicylate and dried onto filter paper for fluorography. Electronic autoradiography was performed on the dried gels using a Packard Instant Imager.

Iodide efflux assay

BHK cells stably expressing wild-type and mutant CFTR grown to ~ 100% confluence in 6 well plates were incubated in an iodide loading buffer (136mM NaI, 3mM KNO_3, 2mM $Ca(NO_3)_2$, 11mM glucose and 20mM HEPES, pH 7.4) for 1 hour at room temperature. Extracellular iodide was removed by rinsing the cells with iodide-free efflux buffer (same as the loading buffer except $NaNO_3$ replaced NaI). Samples were collected by completely replacing the efflux buffer (1 ml volume) with fresh solution at 1 min intervals. The first four samples were used to establish the baseline. An iodide efflux upon stimulation with PKA agonists (10μM forskolin, 100μM dibutyl-cAMP and 1mM 3-isobuty-1-methylxanthine) were measured using an iodide selective electrode LIS-146ICM (Lazar Res. Lab., Inc.), as previously described [48].

Membrane isolation

BHK or HEK 293 cells expressing CFTR variants were harvested by scraping, and homogenized on ice in 10mM HEPES, pH7.2, 1mM EDTA containing a protease inhibitor cocktail (benzamidine at 120 μg ml^{-1}, E64 at 3.5 μg ml^{-1}, aprotinin at 2 μg ml^{-1}, leupeptin at 1 μg ml^{-1} and Pefabloc at 50 μg ml^{-1}). Centrifugation at 600 g for 15 min removed nuclei and undisrupted cells. The supernatant was centrifuged at 100 000 g for 60 min to pellet membranes which were then resuspended in phosphorylation buffer (10mM Hepes, pH 7.2 containing 0.5mM EGTA, 2mM $MgCl_2$, and 250mM sucrose). Brief (3×20 s) bath sonication was used to generate vesicles of uniform size. For the single channel recordings membrane vesicles were phosphorylated by incubation with 50 nM PKA catalytic subunit (Promega) and 2mM Na_2ATP (Sigma) in phosphorylation buffer for 20 min at +4°C. The membranes were aliquoted and stored at −80°C until used.

Photoaffinity labeling

CFTR nucleotide binding and retention assays were performed essentially as described previously [50]. Briefly, membrane suspensions were incubated either at 4°C or 35°C for 5 min with 25μM [γ^{32}P]N_3ATP. The labeled membranes were than UV irradiated directly (Stratalinker UV cross-linker) or after pelleting and washing away unbound nucleotide. To monitor the [γ^{32}P]N_3 ATP dissociation from the nucleotide binding site the washed membranes were resuspended in nucleotide free buffer and UV irradiated after incubation at 35°C for various periods of time. After limited trypsin digestion for 15 min on ice the labeled membranes were solubilized in RIPA buffer and CFTR fragments were immunoprecipitated with mAb13-4 or mAb596. The immunoprecipitates were fractionated by SDS-PAGE (4–20% acrylamide) and transferred on to nitrocellulose membranes for autoradiography [X-ray films and Packard Instant Imager (PerkinElmer)] for quantification of ^{32}P radioactivity associated with NBD1- and NBD2-containing bands.

Single channel measurements

Planar lipid bilayers were prepared by painting a 0.2 mm hole drilled in a Teflon cup with a phospholipids solution in n-decane containing a 3:1 mixture of 1-palmitoyl-2-oleoyl-sn-glycero-3-phosphoethanolamine and 1-palmitoyl-2-oleoyl-sn-glycero-3-phosphoserine (Avanti Polar Lipids). The lipid bilayer separated 1.0 ml of solution in the Teflon cup *(cis* side) from 5.0 ml of a solution in an outer glass chamber (*trans* side). Both chambers were magnetically stirred and thermally insulated. Heating and temperature control were established by a Temperature Control System TC2BIP (Cell Micro Controls).

CFTR ion channels were transferred into the preformed lipid bilayer by spontaneous fusion of membrane vesicles containing CFTR variants. To maintain uniform orientation and functional activity of CFTR channels transferred into the bilayer 2mM ATP, 50 nM PKA and membrane vesicles were added in the *cis* compartment only. All measurements were done in symmetrical salt solution (300 mM Tris/HCl; pH7.2; 3 mM $MgCl_2$ and 1 mM EGTA) under voltage-clamp conditions by using an Axopatch 200B amplifier. The membrane voltage potential of −75 mV is the difference between *cis* and *trans* (ground) compartments. The data analysis was performed as described before [51].

Discrete molecular dynamics (DMD) simulations

Equilibrium DMD simulations [32]; [33] of wild type, ΔF508 and ΔF508-ΔRI CFTR NBD1 were performed for 10^5 DMD time units (approximately 5 ns). The initial co-ordinates were obtained from the crystal structure of NBD1 (PDB: 2BBO and 2BBT) and the system was pre-relaxed before performing long simulations. In order to obtain the dynamic coupling pattern of structurally distant regions, free simulations were performed without holding any part of the protein fixed during the simulations. The dynamic coupling of different constructs of NBD1 was obtained by computing normalized correlation matrices [52]; [53] from DMD simulation trajectories. In the calculation of root mean square fluctuations (RMSF) of each residue in NBD1 over the course of the simulation, the translational and rotational freedom were reduced by translating the center of mass of the protein to the origin before aligning each snapshot with respect to the average structure.

Statistical Analysis

Results are presented as mean value ± SEM. Statistical significances were calculated by using Student's T- test. P values of less than 0.05 were considered significant.

Supplementary Material

Refer to Web version on PubMed Central for supplementary material.

Acknowledgments

This work was supported by grants from the NIH to JRR (DK051870) and NVD (GM080742) and from the Cystic Fibrosis Foundation. We thank Dr. Adrian W. R. Serohijos for useful discussions and preliminary DMD simulations of RI impact on NBD1 dynamics.

Abbreviations used

CFTR	cystic fibrosis transmembrane conductance regulator
CF	cystic fibrosis
NBD1	N-terminal nucleotide binding domain
CL	cytoplasmic loop
RI	regulatory insertion
ER	endoplasmic reticulum
SDR	structurally diverse region
DMD	discrete molecular dynamics
ABC	ATP-binding cassette proteins
RMSF	root-mean-square fluctuations
MSD2	C-terminal membrane spanning domain
VRT-325	4-Cyclohexyloxy-2-{1-[4-(4-methoxy-benzensulfonyl)-piperazin-1-yl]-ethyl}-quinazolin

Corr-4a	N-[2-(5-Chloro-2-methoxy-phenylamino)-4′-methyl-[4,5′]bithiazolyl-2′-yl]-benzamide

References

1. Aleksandrov AA, Aleksandrov LA, Riordan JR. CFTR (ABCC7) is a hydrolyzable-ligand-gated channel. Pflugers Arch. 2007; 453:693–702. [PubMed: 17021796]
2. Wang W, Wu J, Bernard K, Li G, Wang G, Bevensee MO, Kirk KL. ATP-independent CFTR channel gating and allosteric modulation by phosphorylation. Proc Natl Acad Sci U S A. 2010; 107:3888–93. [PubMed: 20133716]
3. Riordan JR. CFTR Function and Prospects for Therapy. Annu Rev Biochem. 2008; 77:701–26. [PubMed: 18304008]
4. Denning GM, Anderson MP, Amara JF, Marshall J, Smith AE, Welsh MJ. Processing of mutant cystic fibrosis transmembrane conductance regulator is temperature-sensitive. Nature. 1992; 358:761–764. [PubMed: 1380673]
5. Howard M, Fischer H, Roux J, Santos BC, Gullans SR, Yancey PH, Welch WJ. Mammalian osmolytes and S-nitrosoglutathione promote Delta F508 cystic fibrosis transmembrane conductance regulator (CFTR) protein maturation and function. J Biol Chem. 2003; 278:35159–67. [PubMed: 12837761]
6. Wang X, Koulov AV, Kellner WA, Riordan JR, Balch WE. Chemical and biological folding contribute to temperature-sensitive DeltaF508 CFTR trafficking. Traffic. 2008; 9:1878–93. [PubMed: 18764821]
7. Pedemonte N, Lukacs GL, Du K, Caci E, Zegarra-Moran O, Galietta LJ, Verkman AS. Small-molecule correctors of defective DeltaF508-CFTR cellular processing identified by high-throughput screening. J Clin Invest. 2005; 115:2564–71. [PubMed: 16127463]
8. Pissarra LS, Farinha CM, Xu Z, Schmidt A, Thibodeau PH, Cai Z, Thomas PJ, Sheppard DN, Amaral MD. Solubilizing mutations used to crystallize one CFTR domain attenuate the trafficking and channel defects caused by the major cystic fibrosis mutation. Chem Biol. 2008; 15:62–9. [PubMed: 18215773]
9. Teem JL, Berger HA, Ostedgaard LS, Rich DP, Tsui LC, Welsh MJ. Identification of revertants for the cystic fibrosis DF508 mutation using STE6-CFTR chimeras in yeast. Cell. 1993; 73:335–346. [PubMed: 7682896]
10. DeCarvalho AC, Gansheroff LJ, Teem JL. Mutations in the nucleotide binding domain 1 signature motif region rescue processing and functional defects of cystic fibrosis transmembrane conductance regulator delta f508. J Biol Chem. 2002; 277:35896–905. [PubMed: 12110684]
11. Serohijos AW, Hegedus T, Aleksandrov AA, He L, Cui L, Dokholyan NV, Riordan JR. Phenylalanine-508 mediates a cytoplasmic-membrane domain contact in the CFTR 3D structure crucial to assembly and channel function. Proc Natl Acad Sci U S A. 2008; 105:3256–61. [PubMed: 18305154]
12. Lewis HA, Zhao X, Wang C, Sauder JM, Rooney I, Noland BW, Lorimer D, Kearins MC, Conners K, Condon B, Maloney PC, Guggino WB, Hunt JF, Emtage S. Impact of the deltaF508 mutation in first nucleotide-binding domain of human cystic fibrosis transmembrane conductance regulator on domain folding and structure. J Biol Chem. 2005; 280:1346–53. [PubMed: 15528182]
13. Qu BH, Strickland EH, Thomas PJ. Localization and suppression of a kinetic defect in cystic fibrosis transmembrane conductance regulator folding. J Biol Chem. 1997; 272:15739–44. [PubMed: 9188468]
14. Serohijos AW, Hegedus T, Riordan JR, Dokholyan NV. Diminished self-chaperoning activity of the DeltaF508 mutant of CFTR results in protein misfolding. PLoS Comput Biol. 2008; 4:e1000008. [PubMed: 18463704]
15. Lewis HA, Buchanan SG, Burley SK, Conners K, Dickey M, Dorwart M, Fowler R, Gao X, Guggino WB, Hendrickson WA, Hunt JF, Kearins MC, Lorimer D, Maloney PC, Post KW, Rajashankar KR, Rutter ME, Sauder JM, Shriver S, Thibodeau PH, Thomas PJ, Zhang M, Zhao X,

Emtage S. Structure of nucleotide-binding domain 1 of the cystic fibrosis transmembrane conductance regulator. EMBO J. 2004; 23:282–93. [PubMed: 14685259]

16. Csanady L, Chan KW, Nairn AC, Gadsby DC. Functional roles of nonconserved structural segments in CFTR's NH2-terminal nucleotide binding domain. J Gen Physiol. 2005; 125:43–55. [PubMed: 15596536]
17. Atwell S, Brouillette CG, Conners K, Emtage S, Gheyi T, Guggino WB, Hendle J, Hunt JF, Lewis HA, Lu F, Protasevich II, Rodgers LA, Romero R, Wasserman SR, Weber PC, Wetmore D, Zhang FF, Zhao X. Structures of a minimal human CFTR first nucleotide-binding domain as a monomer, head-to-tail homodimer, and pathogenic mutant. Protein Eng Des Sel. 2010; 23:375–384. [PubMed: 20150177]
18. Yang H, Shelat AA, Guy RK, Gopinath VS, Ma T, Du K, Lukacs GL, Taddei A, Folli C, Pedemonte N, Galietta LJ, Verkman AS. Nanomolar affinity small molecule correctors of defective Delta F508-CFTR chloride channel gating. J Biol Chem. 2003; 278:35079–85. [PubMed: 12832418]
19. Du K, Sharma M, Lukacs GL. The DeltaF508 cystic fibrosis mutation impairs domain-domain interactions and arrests post-translational folding of CFTR. Nat Struct Mol Biol. 2005; 12:17–25. [PubMed: 15619635]
20. Aleksandrov L, Aleksandrov AA, Chang XB, Riordan JR. The First Nucleotide Binding Domain of Cystic Fibrosis Transmembrane Conductance Regulator Is a Site of Stable Nucleotide Interaction, whereas the Second Is a Site of Rapid Turnover. J Biol Chem. 2002; 277:15419–25. [PubMed: 11861646]
21. Basso C, Vergani P, Nairn AC, Gadsby DC. Prolonged nonhydrolytic interaction of nucleotide with CFTR's NH2-terminal nucleotide binding domain and its role in channel gating. J Gen Physiol. 2003; 122:333–48. [PubMed: 12939393]
22. Cui L, Aleksandrov L, Hou YX, Gentzsch M, Chen JH, Riordan JR, Aleksandrov AA. The role of cystic fibrosis transmembrane conductance regulator phenylalanine 508 side chain in ion channel gating. J Physiol. 2006; 572:347–58. [PubMed: 16484308]
23. Aleksandrov L, Aleksandrov A, Riordan JR. Mg2+-dependent ATP occlusion at the first nucleotide-binding domain (NBD1) of CFTR does not require the second (NBD2). Biochem J. 2008; 416:129–36. [PubMed: 18605986]
24. He L, Aleksandrov AA, Serohijos AW, Hegedus T, Aleksandrov LA, Cui L, Dokholyan NV, Riordan JR. Multiple membrane-cytoplasmic domain contacts in the cystic fibrosis transmembrane conductance regulator (CFTR) mediate regulation of channel gating. J Biol Chem. 2008; 283:26383–90. [PubMed: 18658148]
25. Dalemans W, Barbry P, Champigny G, Jallat S, Dott K, Dreyer D, Crystal RG, Pavirani A, Lecocq JP, Lazdunski M. Altered Chloride-Ion Channel Kinetics Associated with the Delta-F508 Cystic-Fibrosis Mutation. Nature. 1991; 354:526–528. [PubMed: 1722027]
26. Haws CM, Nepomuceno IB, Krouse ME, Wakelee H, Law T, Xia Y, Nguyen H, Wine JJ. DeltaF508-CFTR channels: kinetics, activation by forskolin, and potentiation by xanthines. American Journal of Physiology. 1996; 270:C1544–C1555. [PubMed: 8967457]
27. Schultz BD, Frizzell RA, Bridges RJ. Rescue of dysfunctional deltaF508-CFTR chloride channel activity by IBMX. J Membr Biol. 1999; 170:51–66. [PubMed: 10398760]
28. Wang F, Zeltwanger S, Hu S, Hwang TC. Deletion of phenylalanine 508 causes attenuated phosphorylation-dependent activation of CFTR chloride channels. J Physiol. 2000; 524(Pt 3):637–48. [PubMed: 10790148]
29. Hegedus T, Aleksandrov A, Cui L, Gentzsch M, Chang XB, Riordan JR. F508del CFTR with two altered RXR motifs escapes from ER quality control but its channel activity is thermally sensitive. Biochim Biophys Acta. 2006; 1758:565–72. [PubMed: 16624253]
30. Jurkuvenaite A, Chen L, Bartoszewski R, Goldstein R, Bebok Z, Matalon S, Collawn JF. Functional stability of rescued delta F508 cystic fibrosis transmembrane conductance regulator in airway epithelial cells. Am J Respir Cell Mol Biol. 2010; 42:363–72. [PubMed: 19502384]
31. Van Goor F, Straley KS, Cao D, Gonzalez J, Hadida S, Hazlewood A, Joubran J, Knapp T, Makings LR, Miller M, Neuberger T, Olson E, Panchenko V, Rader J, Singh A, Stack JH, Tung R, Grootenhuis PD, Negulescu P. Rescue of DeltaF508-CFTR trafficking and gating in human cystic

fibrosis airway primary cultures by small molecules. Am J Physiol Lung Cell Mol Physiol. 2006; 290:L1117–30. [PubMed: 16443646]

32. Dokholyan NV, Buldyrev SV, Stanley HE, Shakhnovich EI. Discrete molecular dynamics studies of the folding of a protein-like model. Fold Des. 1998; 3:577–87. [PubMed: 9889167]
33. Ding F, Dokholyan NV. Emergence of protein fold families through rational design. PLoS Comput Biol. 2006; 2:e85. [PubMed: 16839198]
34. Kanelis V, Hudson RP, Thibodeau PH, Thomas PJ, Forman-Kay JD. NMR evidence for differential phosphorylation-dependent interactions in WT and DeltaF508 CFTR. Embo J. 2010; 29:263–77. [PubMed: 19927121]
35. Lewis HA, Wang C, Zhao X, Hamuro Y, Conners K, Kearins MC, Lu F, Sauder JM, Molnar KS, Coales SJ, Maloney PC, Guggino WB, Wetmore DR, Weber PC, Hunt JF. Structure and Dynamics of NBD1 from CFTR Characterized Using Crystallography and Hydrogen/Deuterium Exchange Mass Spectrometry. J Mol Biol. 2010; 396:406–430. [PubMed: 19944699]
36. Schmitt L, Benabdelhak H, Blight MA, Holland IB, Stubbs MT. Crystal structure of the nucleotide-binding domain of the ABC-transporter haemolysin B: identification of a variable region within ABC helical domains. J Mol Biol. 2003; 330:333–42. [PubMed: 12823972]
37. Ward CL, Omura S, Kopito RR. Degradation of CFTR by the ubiquitin-proteasome pathway. Cell. 1995; 83:121–127. [PubMed: 7553863]
38. Jensen TJ, Loo MA, Pind S, Williams DB, Goldberg AL, Riordan JR. Multiple proteolytic systems, including the proteasome, contribute to CFTR processing. Cell. 1995; 83:129–135. [PubMed: 7553864]
39. Sharma M, Pampinella F, Nemes C, Benharouga M, So J, Du K, Bache KG, Papsin B, Zerangue N, Stenmark H, Lukacs GL. Misfolding diverts CFTR from recycling to degradation: quality control at early endosomes. J Cell Biol. 2004; 164:923–33. [PubMed: 15007060]
40. Grove DE, Rosser MF, Ren HY, Naren AP, Cyr DM. Mechanisms for rescue of correctable folding defects in CFTRDelta F508. Mol Biol Cell. 2009; 20:4059–69. [PubMed: 19625452]
41. Wang X, Venable J, LaPointe P, Hutt DM, Koulov AV, Coppinger J, Gurkan C, Kellner W, Matteson J, Plutner H, Riordan JR, Kelly JW, Yates JR 3rd, Balch WE. Hsp90 cochaperone Aha1 downregulation rescues misfolding of CFTR in cystic fibrosis. Cell. 2006; 127:803–15. [PubMed: 17110338]
42. Wang Y, Loo TW, Bartlett MC, Clarke DM. Correctors promote maturation of cystic fibrosis transmembrane conductance regulator (CFTR)-processing mutants by binding to the protein. J Biol Chem. 2007; 282:33247–51. [PubMed: 17911111]
43. Mornon JP, Lehn P, Callebaut I. Molecular models of the open and closed states of the whole human CFTR protein. Cell Mol Life Sci. 2009; 66:3469–86. [PubMed: 19707853]
44. Wang Y, Loo TW, Bartlett MC, Clarke DM. Additive effect of multiple pharmacological chaperones on maturation of CFTR processing mutants. Biochem J. 2007; 406:257–63. [PubMed: 17535157]
45. Loo TW, Bartlett MC, Clarke DM. Introduction of the most common cystic fibrosis mutation (Delta F508) into human P-glycoprotein disrupts packing of the transmembrane segments. J Biol Chem. 2002; 277:27585–8. [PubMed: 12070134]
46. Buyse F, Vandenbranden M, Ruysschaert JM. Mistargeted MRPdeltaF728 mutant is rescued by intracellular GSH. FEBS Lett. 2004; 578:145–51. [PubMed: 15581632]
47. Cui L, Aleksandrov L, Chang XB, Hou YX, He L, Hegedus T, Gentzsch M, Aleksandrov A, Balch WE, Riordan JR. Domain interdependence in the biosynthetic assembly of CFTR. J Mol Biol. 2007; 365:981–94. [PubMed: 17113596]
48. Chang XB, Tabcharani JA, Hou YX, Jensen TJ, Kartner N, Alon N, Hanrahan JW, Riordan JR. Protein kinase A (PKA) still activates CFTR chloride channel after mutagenesis of all ten PKA consensus phosphorylation sites. J Biol Chem. 1993; 268:11304–11311. [PubMed: 7684377]
49. Loo MA, Jensen TJ, Cui L, Hou Y, Chang XB, Riordan JR. Perturbation of Hsp90 interaction with nascent CFTR prevents its maturation and accelerates its degradation by the proteasome. EMBO J. 1998; 17:6879–6887. [PubMed: 9843494]

50. Aleksandrov L, Mengos A, Chang X, Aleksandrov A, Riordan JR. Differential interactions of nucleotides at the two nucleotide binding domains of the cystic fibrosis transmembrane conductance regulator. J Biol Chem. 2001; 276:12918–23. [PubMed: 11279083]

51. Aleksandrov AA, Cui L, Riordan JR. Relationship between nucleotide binding and ion channel gating in cystic fibrosis transmembrane conductance regulator. J Physiol. 2009; 587:2875–86. [PubMed: 19403599]

52. Sharma S, Ding F, Dokholyan NV. Multiscale modeling of nucleosome dynamics. Biophys J. 2007; 92:1457–70. [PubMed: 17142268]

53. Teotico DG, Frazier ML, Ding F, Dokholyan NV, Temple BR, Redinbo MR. Active nuclear receptors exhibit highly correlated AF-2 domain motions. PLoS Comput Biol. 2008; 4:e1000111. [PubMed: 18617990]

54. Glozman R, Okiyoneda T, Mulvihill CM, Rini JM, Barriere H, Lukacs GL. N-glycans are direct determinants of CFTR folding and stability in secretory and endocytic membrane traffic. J Cell Biol. 2009; 184:847–62. [PubMed: 19307599]

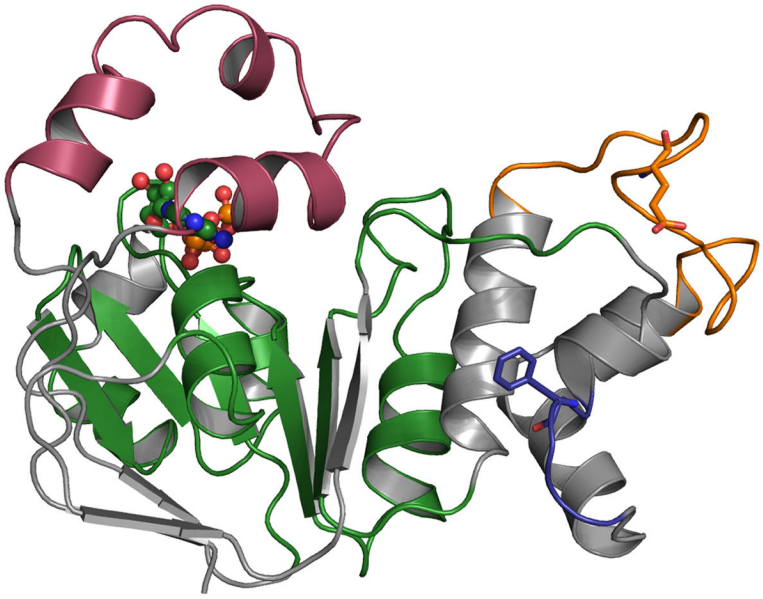

Fig 1. Structural features of wild type CFTR-NBD1

The structure of CFTR NBD1 (PDB: 2BBO) is shown. F1-like ATP binding core sub domain (G451-L475, D565-Q637) and γ-switch (Q493-P499) are in green. The RI region of NBD1 is colored red. ATP is shown in ball and stick representation. The 507–511 loop is colored blue and the side chain of F508 is shown in ball and stick representation. The 536–550 SDR loop is colored orange. Loops are rendered thicker than normal for easier visualization.

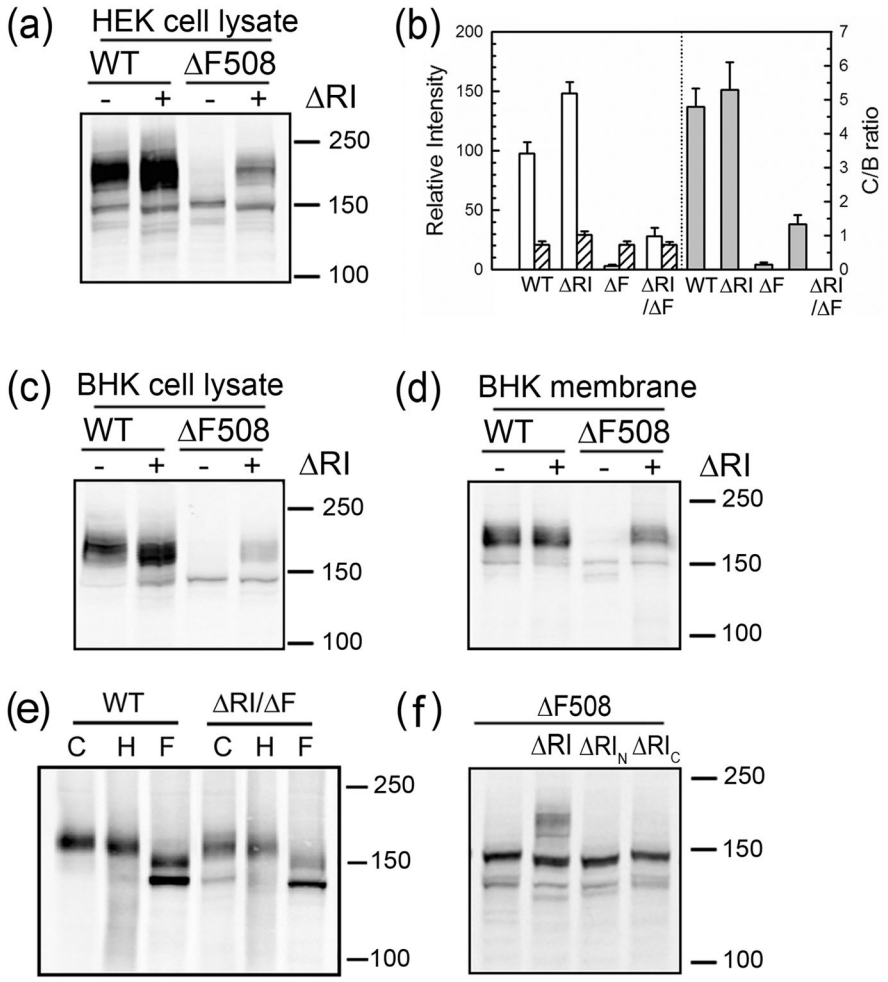

Fig 2. Deletion of RI promotes maturation of ΔF508 CFTR

(a) Cell lysates containing 50 μg of total protein from transiently transfected HEK 293 cells was subjected to Western blot analysis using anti-CFTR antibody mAb596. **(b)** The relative intensities of both mature and immature bands normalized to the wild type CFTR mature band and ratio of mature to immature band intensities are shown. The open and hatched bars represent mature and immature bands respectively. The gray bars on the right represent the ratio of mature to immature bands intensities. All data are shown as mean value ± SEM from 3 independent experiments. Western blots (mAb596) of cell lysates with 50 μg of total protein are shown in **(c)** and membranes with 10 μg of total protein in **(d)** from BHK cells stably expressing CFTR variants. **(e)** Membrane vesicles prepared from BHK cells expressing WT- and ΔRI/ΔF508-CFTR were treated with endoglycosidase H or N-glycanase F before subjecting to Western blot analysis. Note that N-glycanase digestion results in two bands of higher mobility, the smaller representing the completely deglycosylated protein from which both N-linked chains have been removed and the larger intermediate band, the product with only the more susceptible chain removed. C-control; H-endoglycosidase H; F-N-glycanase F. **(f)** Western blots (mAb596) of HEK 293 cells transiently transfected with ΔF508-CFTR with the entire RI (ΔRI), N-terminal portion (ΔRI_N) or C-terminal portion

(ΔRI_C) deleted. ΔRI_N and ΔRI_C refers to the deletion of RI fragments 404–412 and 414–432 respectively.

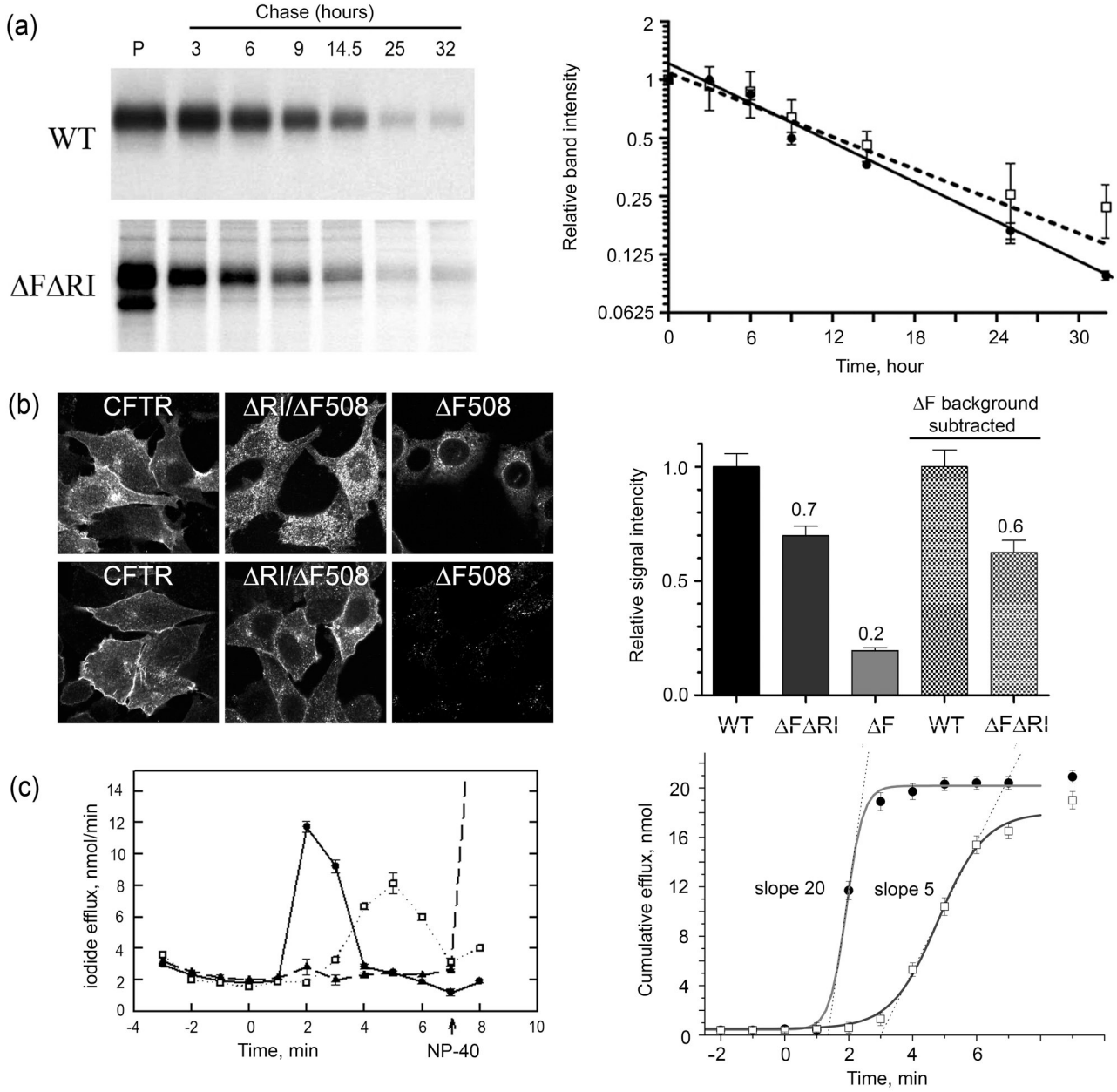

Fig 3. Deletion of RI promotes maturation, life time on the cell surface and function of ΔF508 CFTR

(a) Wild type and ΔRI/ΔF508 CFTR cells were pulsed with [^{35}S]-methionine for 8 hours and the disappearance of the mature protein was followed during a 32 hour chase. Quantification of the bands and single exponential fit for both the wild type and ΔRI/ΔF508 CFTR in the graph to the right show that the two have similar turnover kinetics with a $T_{1/2}$ of ~12 hours for wild type (solid circle, solid line) and ~14 hours for the mutant (open square, dashed line). Each experimental point is shown as a mean value ± SEM from 3 independent experiments. **(b)** Immunofluorescence microscopy of BHK cells stably expressing wild-type, ΔRI/ΔF508 and ΔF508 CFTR was performed on fixed and permeabilized cells using anti-CFTR mouse monoclonal antibody 570, followed by goat

anti-mouse IgG Alexa Fluor 488 conjugate (upper row). Cells also were treated with 100 μM cycloheximide for 4hrs before immunostaining to deplete the intracellular pool of immature protein (bottom row). The cycloheximide treated cells were used to estimate surface density of CFTR variants by quantifying the fluorescence intensity. Using ImageJ, a 250×250 pixel square was defined and the average pixel intensity within measured. Then the region was moved to cover several cells per image and several images were measured per each variant (WT n=61, ΔRI/ΔF508 n=74, ΔF508 n=41). The background was measured from several cell free areas of the individual images and subtracted from the cell measurements to correct for variations in image brightness between images. Measurements were normalized to the WT average value and shown on the graph at the right (3 bars from the left). Since a 3h cycloheximide treatment can clear ΔF508 CFTR signal from a Western blot [39]; [54], our 4h treatment should have been sufficient. The residual signal seen in the ΔF508 CFTR images probably represents degradation products that are still detectable. The two bars on the right represent relative intensities when ΔF508 CFTR background is subtracted. **(c)** CFTR channel activity measured by iodide efflux assay using BHK cells expressing wild-type CFTR (solid circles, solid line), ΔRI/ΔF508 CFTR (open square, dotted line) or ΔF508 CFTR (solid triangle, dashed line). Cells were loaded with iodide and efflux was measured using an iodide selective electrode. The stimulation cocktail was added at time 0 to activate efflux through CFTR channels. The values represent the mean ± SEM of the amount of iodide released from the cells during each 1 min interval (n=3). At the end of each assay, efflux buffer containing 0.1% NP40 was added (arrow) to release retained iodide. These efflux data were transformed to yield the cumulative iodide efflux graph on the right. This provides a numerical estimation of cellular membrane permeabilities. The maximum slope of the tangent line to the best fit of the data set is a reasonable estimation of the maximum value of efflux $J \sim NP_o$. The ratio of maximum slopes $(J_{\Delta RI/\Delta F508})/(J_{wt}) \approx (NP_o)_{\Delta RI/\Delta F508}/(NP_o)_{wt} \approx 5/20 = 0.25$. If the ratio of $(P_o)_{\Delta RI/\Delta F508}/(P_o)_{wt}$ is about 0.5 (Fig. 7a,8a), then $N_{\Delta RI/\Delta F508}/N_{wt} = 0.5$ is an upper estimate. Nearly identical values of the total efflux for the wild type and ΔRI/ΔF508 CFTR after cells solubilization by NP-40 (indicated by symbols separated from the curves) provide evidence of similar iodide loading of similar numbers of cells.

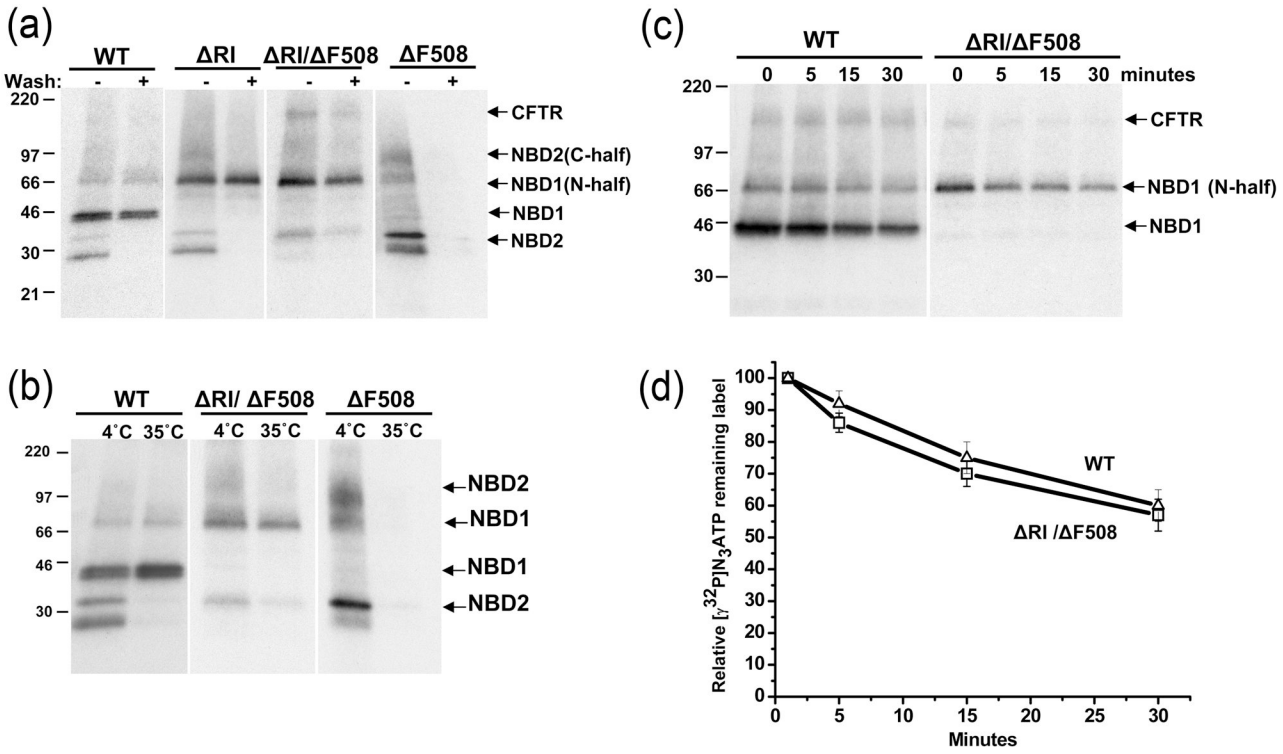

Fig 4. ATP binding and occlusion by ΔF508 CFTR at 35°C is restored upon RI deletion

(a) Membranes from BHK cells expressing wild-type or mutant CFTR after $8N_3[\gamma^{32}P]ATP$ binding at 4°C were UV irradiated before or after washing away free radioactive nucleotide as indicated. After limited trypsin digestion and solubilization in RIPA buffer the tryptic fragments were immunoprecipitated with monoclonal antibodies 13–4 and 596, resolved by SDS-PAGE (4–20% acrylamide) and subjected to autoradiography. **(b)** Membrane proteins after incubation with $8N_3[\gamma^{32}P]ATP$ at 4°C or 35°C for 5 minutes were UV irradiated and treated as in (a). **(c)** Membranes from cells expressing wild-type and mutant CFTR were incubated with $8N_3[\gamma^{32}P]ATP$ and free nucleotide was washed away. The membrane pellets were resuspended in nucleotide free buffer and samples were UV-irradiated after incubation at 35 C for the indicated periods. The photo-labeled proteins were digested and analyzed as in (a) but using only mAb 13–4. **(d)** Quantification of autoradiogram from (c) by electronic radiography.

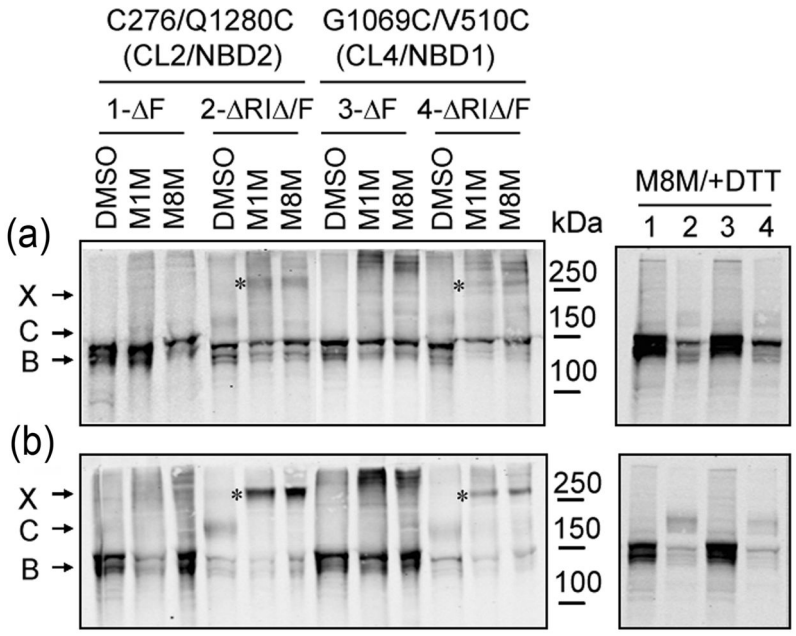

Fig 5. Restoration of MSD/NBD interfaces by RI deletion from ΔF508 CFTR

HEK293 cells were transiently transfected with Cys-less ΔF508 CFTR with Cys-pairs introduced at the CL2/NBD2 (C276/Q1280C) or CL4/NBD1 (V510C/G1069C) interfaces in the absence or presence of ΔRI. Twenty-four hours after transfection, cells were grown for a further 24 hours at 37°C **(a)** or 27°C **(b).** Cells were harvested and washed, and cross-linking of Cys-pairs with 200 μM of MTS cross-linkers (M1M and M8M) was carried out as described before[11]. Cell lysates in SDS-PAGE sample buffer with or without DTT as indicated were subjected to Western blot analysis using mAb596. X: cross-linked CFTR (bands also marked by asterisks); C: mature complex-glycosylated CFTR; B: immature core-glycosylated CFTR.

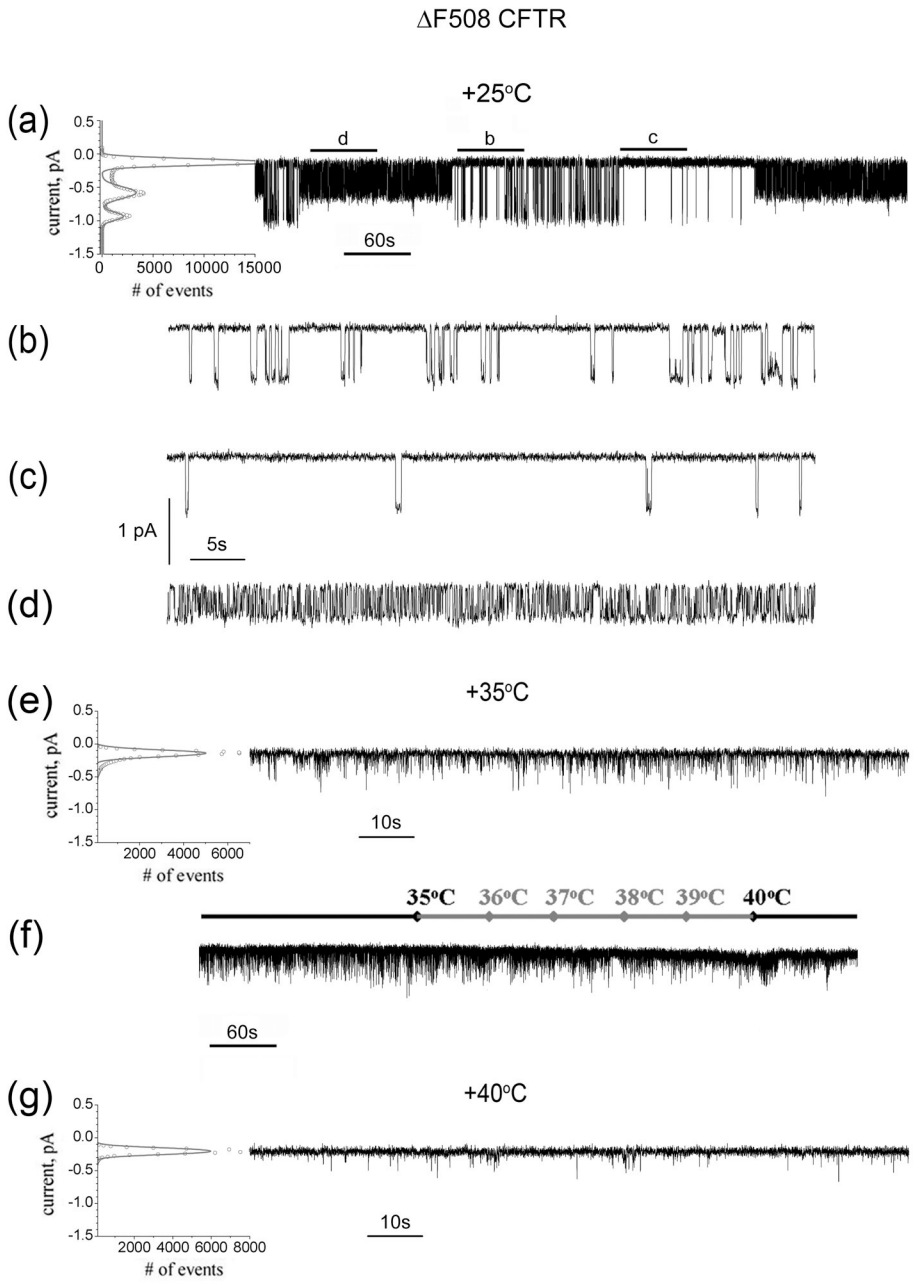

Fig 6. Single channel recordings of ΔF508 CFTR at different temperatures

(a) Ten minute recording of a temperature and corrector rescued ΔF508 CFTR single channel at +25°C. The reversible inter-conversion between patterns of activity with two different conductance of 10.6±0.4 pS and 6.1±0.6 pS was confirmed by two well resolved peaks of open states in the all points histogram shown on the left. The peak values were found from multiple peaks Gaussian fitting and used to calculate conductance and standard deviation. The different patterns of activities in **(a)** are displayed in extended time scale in **(b)**, **(c)** and **(d)**. The locations of these patterns in the entire recording in (a) are marked by solid lines above. **(d)** Only an activity with a stable conductance level of 6.1 pS and P_o=

0.52 was detected after 15 minutes incubation in the experimental chamber at +25°C. **(e)** At +35°C no stable open states were detected while unresolved brief openings still occur and is large in number. **(f)** Further lost of functional ability occurred when the temperature was continuously increased from +35°C to +40°C at a rate of 1°C per minute. **(g)** The residual channel activity with very rare and brief openings was observed at +40°C.

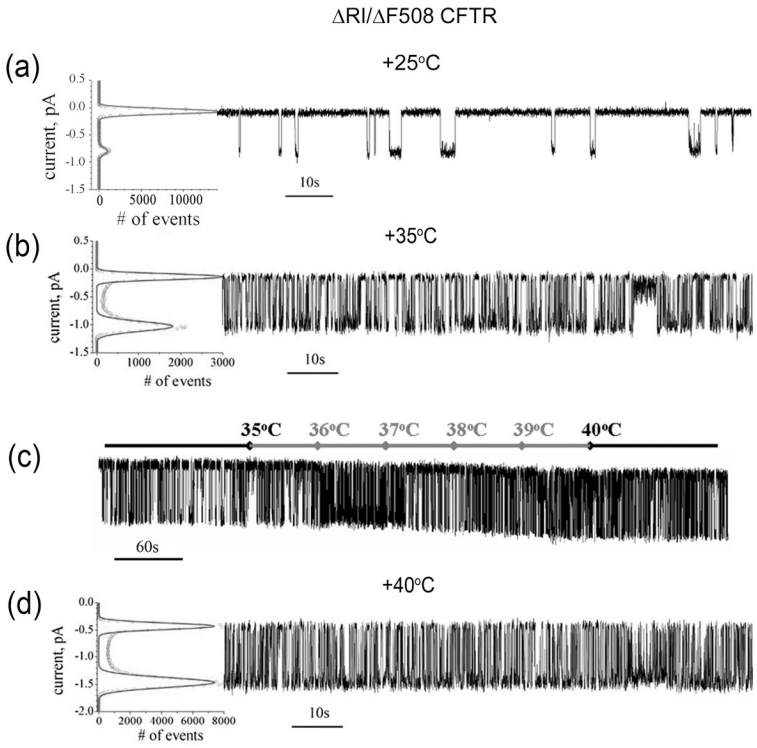

Fig 7. RI deletion stabilizes ΔF508 CFTR channel activity

(a) Two minute recording of a ΔRI/ΔF508 CFTR single channel at +25°C is shown at the right. All points histogram used to calculate P_o and γ is shown at the left. Unlike rescued ΔF508 CFTR, ΔRI/ΔF508 CFTR has stable activity at +25°C with P_o = 0.12±0.03 and γ = 10.6±0.03 pS calculated from 6 independent experiments of 54 minutes total duration. **(b)** All points histogram used to calculate single channel parameters and two minute of ΔRI/ΔF508 CFTR single channel recording at 35°C is shown from left to right. Five independent experiments with total recording time of 42 minutes were used to calculate single channel parameters P_o = 0.53±0.04 and γ = 13.1±0.02 pS.

(c) ΔRI/ΔF508 CFTR single channel recording during continuous temperature increase from +35°C to +40°C. After 3 minutes of recording at +35°C the temperature was increased at a constant rate of 1°C per minute up to +40°C and kept at this temperature for the last two minutes. The current temperature in the chamber was monitored and shown above the trace.

(d) Two minutes of ΔRI/ΔF508 CFTR single channel recording at +40°C is shown on the right. All points histogram used to calculate P_o and γ is shown at the left. Three independent experiments with total recording time of 21 minutes were used to calculate single channel parameters P_o = 0.65±0.03 and γ = 14.1±0.02 pS. All data shown as mean values ± S.E.M

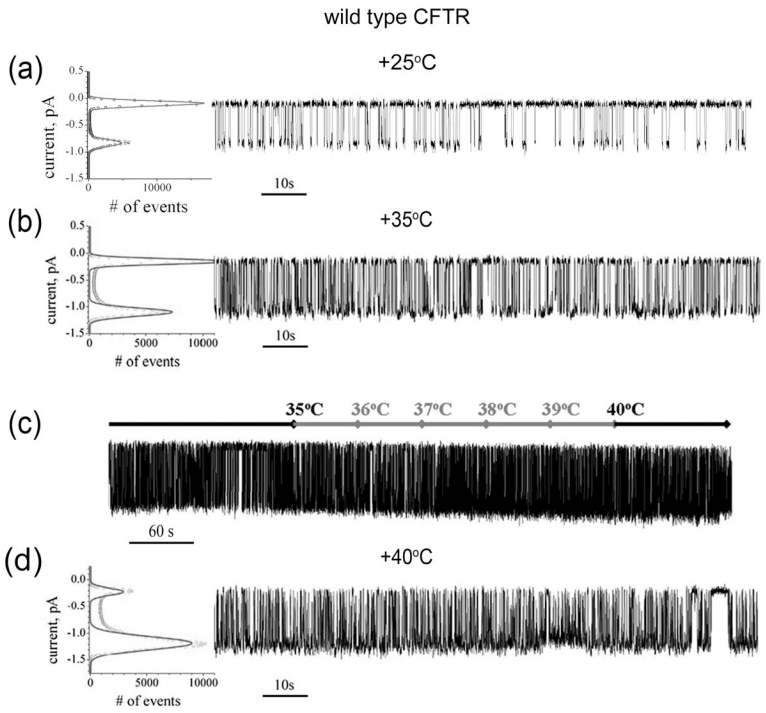

Fig 8. Influence of temperature on wild-type CFTR gating

(a) All points histogram and two minute of wild type CFTR single channel recording at 25°C are shown from left to right. The single channel parameters P_o= 0.26±0.03 and γ = 10.7±0.03 pS were derived from a total recording time of 38 minutes in 4 independent experiments. **(b)** Temperature ramp. After 3 minutes of recording at 35°C the temperature was increased at a constant rate of 1°C per minute up to 40°C and kept at this temperature for the last two minutes. The current temperature in the chamber is shown above the trace. **(c)** All points histogram and two minutes of wild type CFTR single channel recording at 40°C. P_o= 0.74±0.05 and γ = 14.1±0.03 pS. A total recording time of 34 minutes from 4 independent experiments was used to calculate mean values. Data is shown as mean value ± SEM.

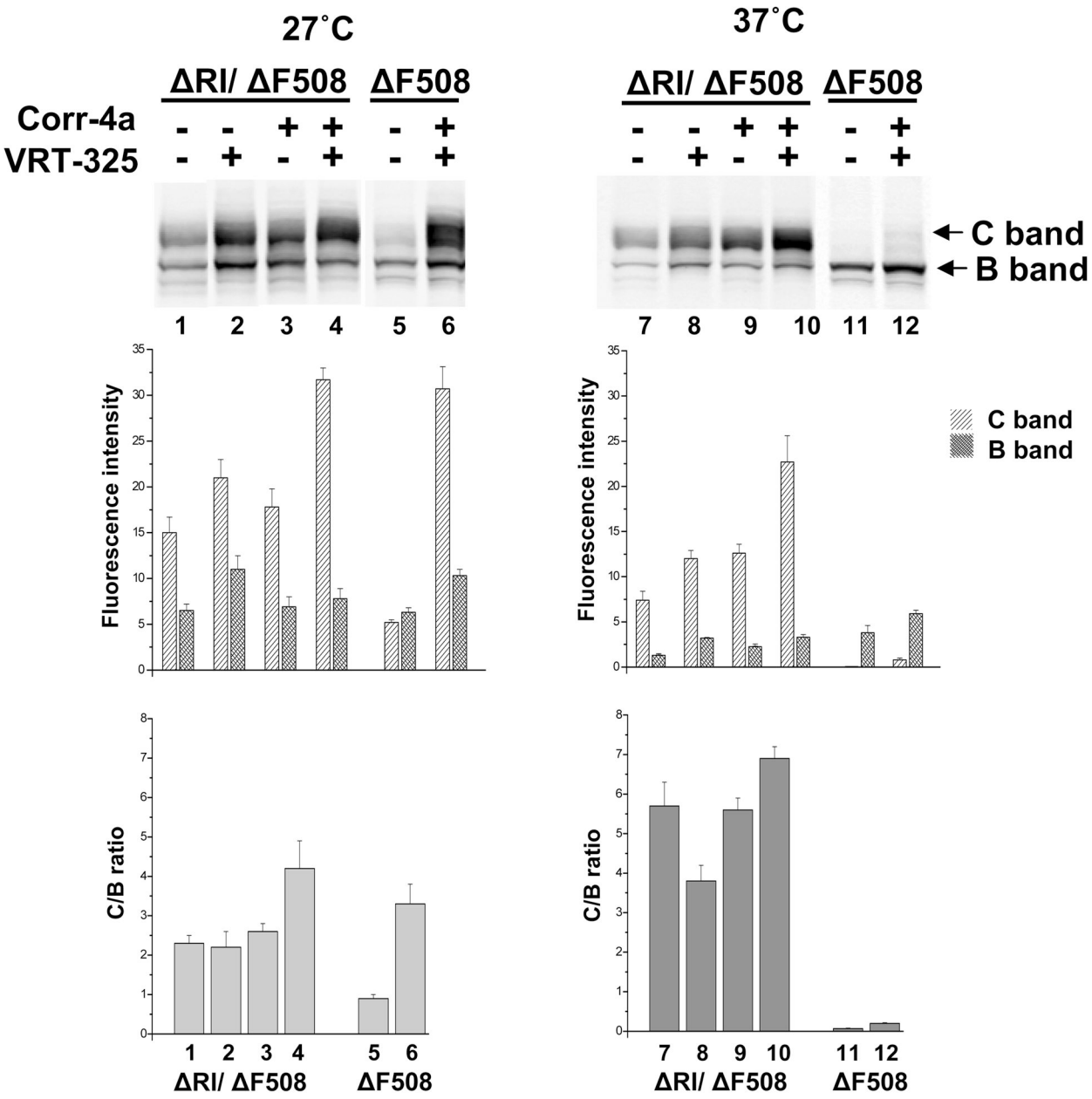

Fig 9. RI deletion and small molecule correctors have additive effects on ΔF508 CFTR maturation

ΔRI/ΔF508 CFTR expressing BHK cells were grown in the presence or absence of 10μM corr-4A or VRT-325 or their combination at 27°C or 37°C for last the 24h before harvesting. Whole cell extracts were then subjected to SDS-PAGE and immunoblot analysis with mAb596. The positions of mature (C) and immature (B) CFTR bands are indicated. The relative fluorescence intensities of these bands as measured at 800 nm in a Li-Cor Odyssey Imager are shown in the bar graphs immediately below the blots and the C band to B band ratios below these.

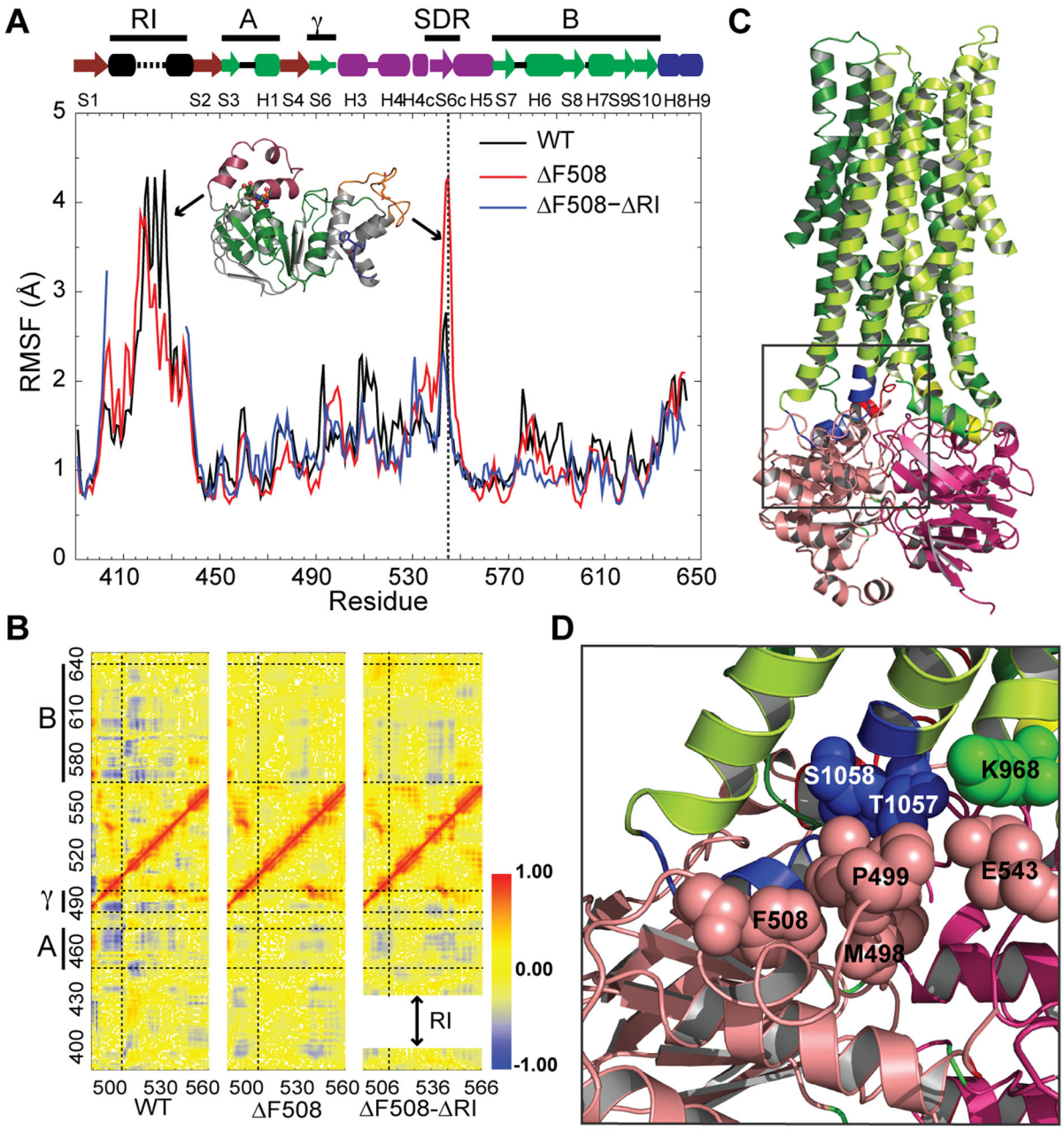

Fig 10. Dynamics of CFTR NBD1 from DMD simulations

(a) Dynamic flexibility of regions in NBD1 was measured as root-mean-square fluctuations (RMSF). The vertical dotted line indicates fluctuations of the loop containing the E543 site. Structural regions corresponding to the peaks in the plot are shown by arrows. Secondary structural elements of NBD1 are represented by the arrows and cylinders above. The two portions of the F1-ATP-binding core subdomain (A:G451-L475 and B:D565-Q637) and γ-switch (Q493-P499) are colored green and labeled by the bold lines at the top for further reference. **(b)** Pairwise correlation map of the velocities of the C_α atoms in the 490–560 region with those of all other segments of NBD1. The regions of the F1-like ATP binding core subdomain (A and B) and γ-switch are marked by bold lines on the left of the Y-axis

and continued throughout the graphs as pairs of horizontal dotted lines. The vertical dotted line shows the position of F508. The shift in the X-axis of the ΔF508-ΔRI correlation map is a consequence of RI deletion. The color code is shown on the right with Red (Correlation coefficient = 1) indicating residue pairs that move in concert in the same direction, and Blue (Correlation coefficient = −1) indicating residue pairs that move with opposite velocity all the time. **(c)** Structural model of full-length CFTR (http://dokhlab.unc.edu/research/CFTR/home.html). The area of the NBD1-CL3-CL4 interface is boxed for further detailed consideration in (d). **(d)** Detailed view of the location and orientation of the residues in the NBD1-CL3-CL4 interface shown inside the box in (c). Residues F508, P499, M498 and E543 from NBD1 (salmon), S1058 and 1057 from CL4 (blue) and K968 from CL3 (cyan) are shown as spheres.